

In-vivo imaging of inner retinal cellular morphology with adaptive optics - optical coherence tomography: challenges and possible solutions

Robert J. Zawadzki^a, Steven M. Jones^b, Dae Yu Kim^a, Lisa Poyneer^b, Arlie G. Capps^{a,c}, Bernd Hamann^c, Scot S. Olivier^b and John S. Werner^a

^aVision Science and Advanced Retinal Imaging Laboratory (VSRI) and Dept. of Ophthalmology & Vision Science, UC Davis, 4860 Y Street, Suite 2400, Sacramento, CA USA 95817;

^bLawrence Livermore National Laboratory, 6000 East Avenue, Livermore, CA USA 94550;

^cInstitute for Data Analysis and Visualization (IDAV), Department of Computer Science, UC Davis, One Shields Avenue, Davis, CA 95616, USA

ABSTRACT

Recent progress in retinal image acquisition techniques, including optical coherence tomography (OCT) and scanning laser ophthalmoscopy (SLO), combined with improved performance of adaptive optics (AO) instrumentation, has resulted in improvement in the quality of *in vivo* images of cellular structures in the outer layers of the human retina. Despite the significant progress in imaging cone and rod photoreceptor mosaics, visualization of cellular structures in the inner retina has been achieved only with extrinsic contrast agents that have not been approved for use with humans. In this paper we describe the main limiting factors in visualizing inner retinal cells and the methods we implemented to reduce their effects on images acquired with AO-OCT. These include improving the system point spread function (AO performance), monitoring of motion artifacts (retinal motion tracking), and speckle pattern reduction (temporal and spatial averaging). Results of imaging inner retinal morphology and the improvement offered by the new UC Davis AO-OCT system with spatio-temporal image averaging are presented.

Keywords: adaptive optics; optical coherence tomography; ophthalmology; imaging systems; medical optics instrumentation; aberration compensation; complex conjugate artifact

1. INTRODUCTION

Over the last two decades, all three retinal imaging modalities that are used in ophthalmic clinics [*i.e.*, fundus camera, scanning laser ophthalmoscope (SLO) and optical coherence tomography (OCT)] have been combined successfully with adaptive optics (AO) making possible imaging of different aspects of retinal morphology and function. The most successful AO instruments have been implemented for *in-vivo* photoreceptor imaging, including recent reports on foveal cones [1,2] and rod photoreceptors [3]. We note that several groups reported imaging of macroscopic inner retinal morphology (in some cases without AO) including capillary beds and nerve fiber layer (NFL) bundles [4,5]. Despite this progress, visualization of the cellular structures in the inner retina has not been achieved.

AO-OCT may have the greatest potential for successful imaging of cellular features in the inner retina due to its high sensitivity and dynamic range [6]. However there are several factors that limit our ability to obtain successful images of inner retinal cells. These include motion artifacts, high speckle contrast, size of the point-spread function (PSF), and the optical properties of inner retinal structures. In this paper, we characterize and reduce the negative effects of the aforementioned factors by using several innovative image acquisition, manipulation and processing techniques.

Briefly, retinal motion artifacts can be reduced by implementation of an AO system that combines an SLO with spectrometer-based Fourier-domain OCT to allow simultaneous data acquisition with two modalities [7] and extraction of retinal motion data from AO-SLO frames to monitor motion artifacts in AO-OCT volumes and line scans.

Speckle contrast is reduced by temporal and spatial averaging. Results of imaging and visualization of inner retinal morphology with the new UC Davis AO-OCT/AO-SLO system is shown on cross sectional B-scans.

*rjzawadzki@ucdavis.edu; phone 1 916 734-4541; fax 1 916 734-4543; <http://vsri.ucdavis.edu/>

2. MATERIALS AND METHODS

The imaging system used to acquire data presented in this manuscript has been developed in the VSRI laboratory over the last several years. Some details on combined AO-OCT/AO-SLO system can be found in our recent Biomedical Optics Express paper [7]. Therefore we will only describe its main characteristics. Briefly, in our AO-OCT/AO-SLO system, the OCT light serves as the beacon for wavefront sensing in the AO sub-system. The light source for OCT in the current configuration is a superluminescent diode (SLD) Broadlighter operating at 836 nm with 112 nm spectral bandwidth (Superlum LTD), allowing 3.5 μm axial resolution at the retina. The light source for the SLO sub-system is also an SLD from Superlum Ltd., operating at 680 nm with 10 nm spectral bandwidth. A pupil diameter of 6.7 mm was used in imaging to allow for up to 3 μm lateral resolution when AO correction is optimized. In the current system configuration we use the whole pupil (13.5mm) of a high stroke 97-actuator ALPAO membrane magnetic deformable mirror. This improves the psf of our AO-OCT system. Light reflected from the sample is combined with the light from the reference mirror, and then sent to a spectrometer where the CCD line detector (SM2, e2V), 14 kHz line rate at 2048 pixels and $14 \times 14 \mu\text{m}$ pixels, acquires the OCT spectrum. B-scan imaging frame rates (frames/s) are 27 fps, for 512 A-scans and 18 fps for 1000 A-scans using 2048 detector pixels. A bite-bar and a forehead-rest assembly have been mounted on a motorized X-Y-Z translation stage to reduce head motion and allow precise positioning of the subject's eye pupil.

2.1. Speckle contrast reduction

Speckles are inherently connected with OCT as this technique uses coherent detection to extract depth scattering profiles from combined sample and reference arm spectra. One of the widely accepted ways of speckle contrast reduction includes averaging of multiple OCT B-scans. This method is supported by some clinical OCT systems and includes frame registration [8] before averaging to reduce unnecessary blurring of retinal features. It is important to average frames that exhibit minimum motion artifacts and that show similar retinal structures. Otherwise, vertical eye motion shifts the B-scans to different retinal locations. These frames are then averaged, i.e., each pixel value is calculated as an average intensity from all frames, to create one frame. Figure 1 illustrates the results of this procedure when using our clinical OCT system (4.5 μm axial resolution) with different numbers of averaged frames.

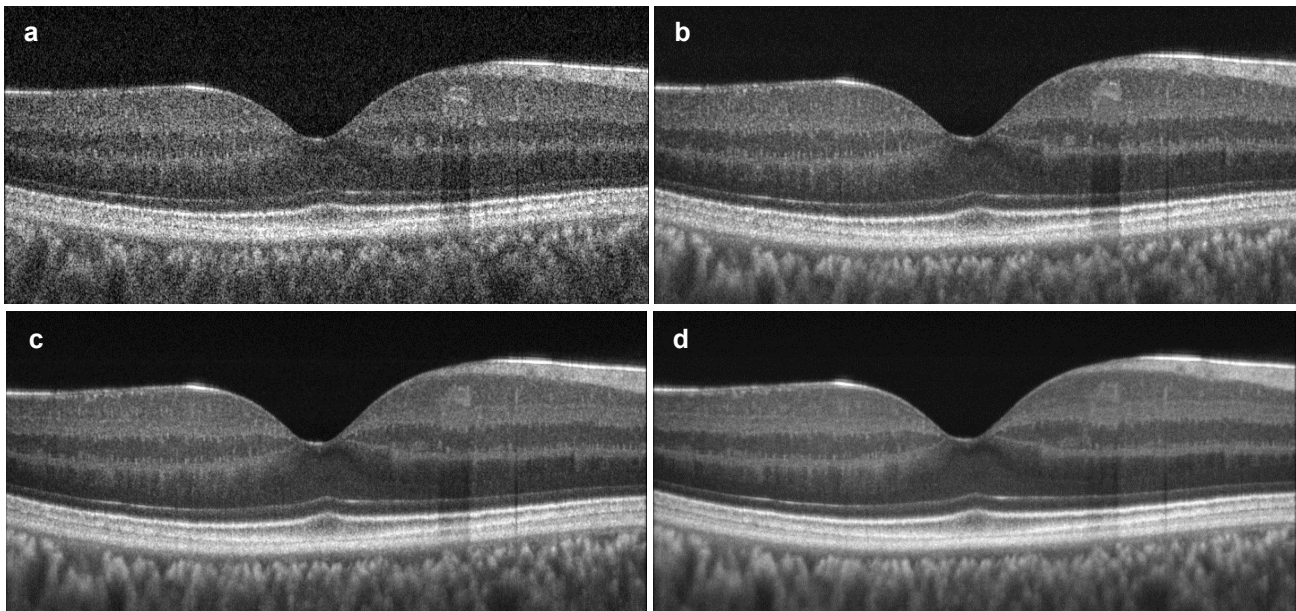


Fig. 1. UHR-OCT B-scan (5mm) acquired with a UC Davis clinical system. a): single frame; b): An average of 10 OCT B-scans; c): An average of 24 OCT B-scans; d): An average of 50 OCT B-scans.

Clear reduction in speckle contrast can be observed between these images. Additionally, contrast reduction is improved with increased number of B-scans. We discuss examples involving data acquired with our AO-OCT in result section of this manuscript.

3. RESULTS

In this section we show the results of tracking retinal motion and describe some consequences for AO-OCT data sets. Then, averaged AO-OCT B-scans are compared to retinal histology images.

3.1. Retinal motion tracking

What is unique in our new approach is the use of motion data derived from SLO images to monitor retinal motion artifacts in OCT volumes, enabling tests of efficiency of spatio-temporal speckle averaging in controlled settings. This allows us to determine what amount of temporal averaging is used for given data sets. Figure 2 shows retinal fixation patterns and true traces of AO-OCT 3D and line scans on the retina after applying motion correction to AO-OCT scanning patterns.

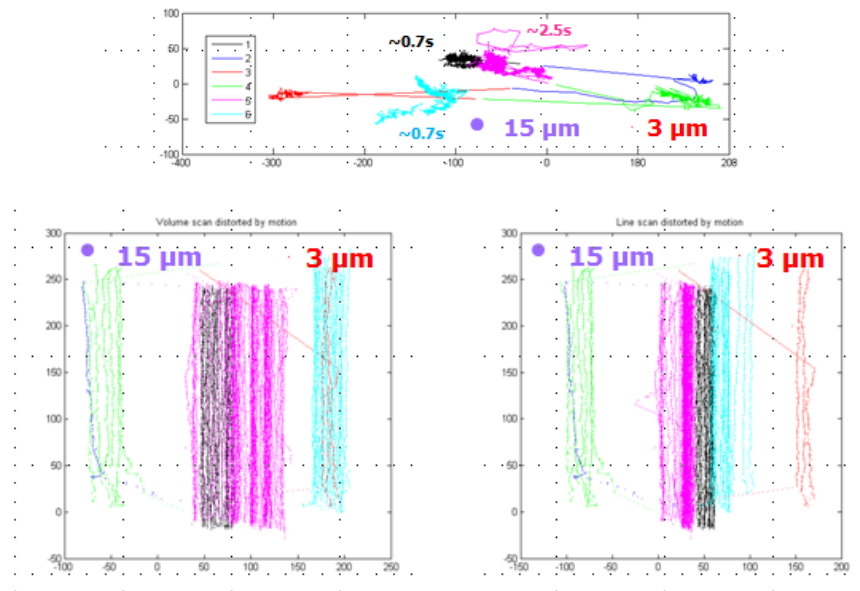


Fig. 2. Results of tracking retinal motion during AO-OCT/AO-SLO data acquisition $T=4.45s$. Top: retina fixation traces during data acquisition; 125 pixels = 1° . Relatively stable fixation periods are marked by the same color and fixation durations for these periods are indicated in the same color. Bottom Left: real traces of the AO-OCT raster during 3D ($2^\circ \times 2^\circ$) acquisition. Bottom Right: real traces of the AO-OCT raster during line acquisition ($\sim 2^\circ$). The standard OCT ($15\mu m$) and AO-OCT / AO-SLO ($3\mu m$) imaging beam spots are marked purple and red, respectively.

Note that relatively large retinal motion during fixation results in sparse and non-uniform sampling of 3D AO-OCT data sets. One can see that when properly chosen OCT B-scans were used for averaging in line acquisition a controlled amount of spatial averaging could be achieved. Therefore we decided to explore line B-scan averaging as a method to enhance our AO-OCT image quality by lowering speckle contrast.

It is worth mentioning that the effect of retinal motion during AO-OCT data acquisition is amplified by a relatively small field of view (FOV) of the AO-OCT data sets. Therefore retinal motion distortion is less relevant when large retinal FOVs are used, which is typically the case for OCT data sets or when ultra-high speed image acquisition is implemented [9] allowing reduction of single volume data acquisition time well below 1s. Figure 3 shows retinal motion traces from Fig. 2 scaled to the $1 \times 1mm$, $5 \times 5mm$ and $10 \times 10mm$ retinal scanning areas that are commonly used in AO-OCT ($1 \times 1mm$) and OCT data acquisition schemes.



Fig. 3. Retina motion traces from Fig. 2 scaled to the 1x1mm, 5x5mm and 10x10mm areas used to acquire AO-OCT and OCT data sets. The OCT beam spot of 15μm is shown for comparison.

This figure also shows why, despite retinal motion artifacts, one can successfully visualize volumetric structures of the retina for OCT data sets. Specifically, in large FOV data acquisition, retinal motion is smaller than scanned retinal features of the retinal morphology of interest. In 3D AO-OCT, due to the retinal motion that might be in the order of the whole scanning range, patients with excellent fixation are needed to obtain meaningful microscopic volumetric morphology.

3.2. Speckle contrast reduction on AO-OCT data sets

Here we present a result of speckle contrast reduction on an AO-OCT data set acquired over a 0.5mm horizontal range. Similarly to OCT B-scan averaging we also have to choose AO-OCT frames that exhibit minimum motion artifacts and that show similar retinal structures. These frames are then averaged, i.e., each pixel value is calculated as an average intensity from all frames. Figure 4 shows results of this averaging for 6, 11 and 20 frames. The reduced number of averaged frames used to produce these images when compared to OCT frame averaging is due to the fact that only a small number of B-scans captured the same retinal features.

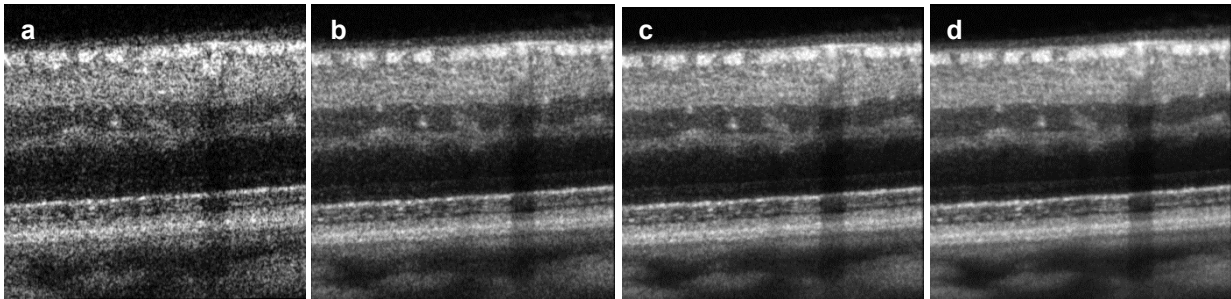


Fig. 4. AO-OCT B-scan (0.5mm) acquired with the UC Davis AO-OCT/AO-SLO system. a): single frame, b): An average of 6 AO-OCT B-scans. c): An average of 11 AO-OCT B-scans. d): An average of 20 AO-OCT B-scans.

Again, clear reduction in speckle contrast can be observed with averaging with an increased number of B-scans.

3.3. Comparison between AO-OCT and OCT data sets

We now compare the results of visualizing 6mm retinal B-scans acquired for the same subject with clinical OCT and AO-OCT systems. Both averages are based on multiple B-scans (15-30), the number depending on motion artifacts present during data acquisition. OCT images were created by averaging B-scans acquired during one OCT line scan acquisition. AO-OCT data was created by stitching 7 AO-OCT averaged B-scans acquired at 7 different retinal eccentricities with AO-OCT line scan acquired over 1mm. For AO-OCT averaging we also chose only frames that exhibit minimal motion artifacts and show similar retinal structures.

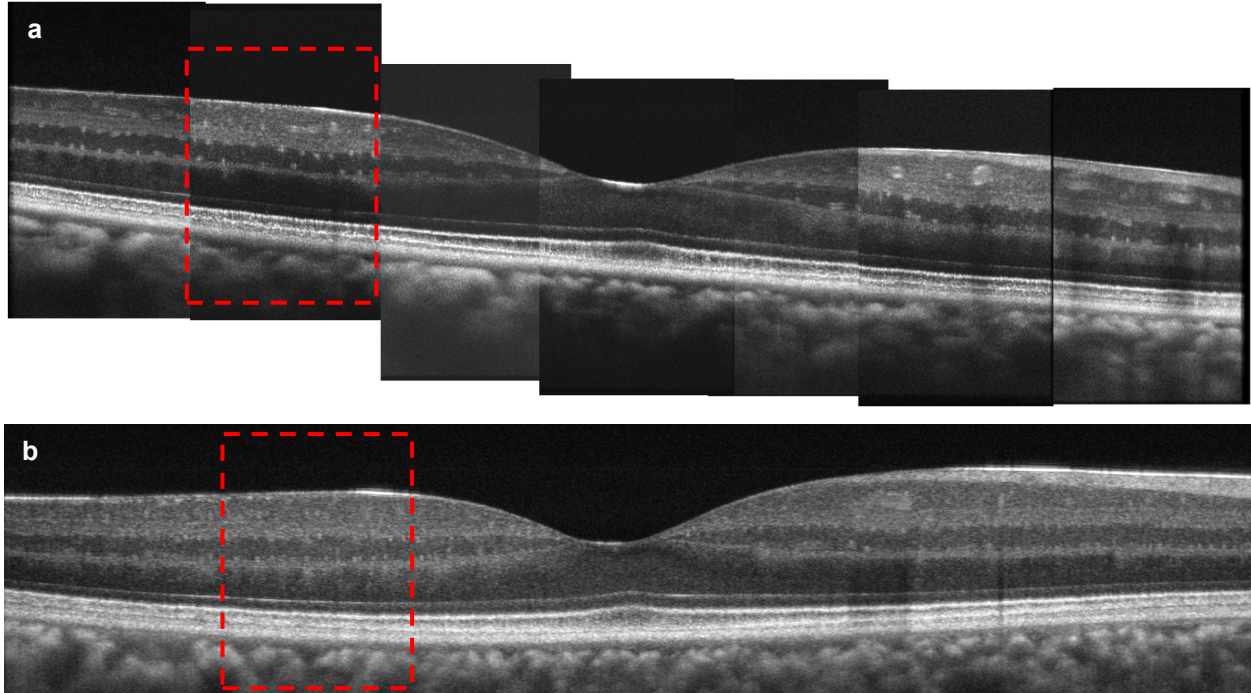


Fig. 5. a) Mosaic of 7 averaged AO-OCT B-scans acquired with the UC Davis AO-OCT/AO-SLO system. b): An average of 25 OCT B-scans acquired with the UC Davis clinical OCT system. The red rectangle points to the area that is compared in Fig. 6.

Note that AO-OCT images offer much more detailed views of retinal structures when compared to OCT averaged B-scans. This is due to improved lateral and axial resolution as well as increased numbers of total A-scans per B-scan (1000 A-scans for averaged OCT-B-scan and ~6,000 A-scans for the mosaic of 7 averaged AO-OCT B-scans).

Figure 6 shows zoomed-in areas of 1mm at about 6° Temporal Retina (TR) from both images. Additionally a histology cross section, with similar magnification, of the inner retina is shown for comparison.

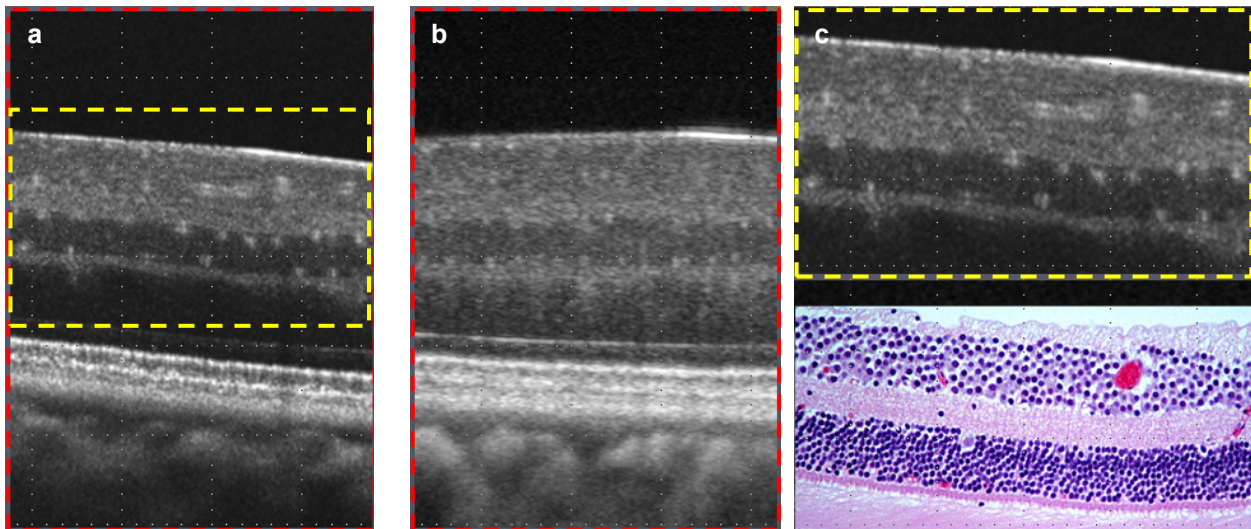


Fig. 6. Comparison between AO-OCT and OCT data sets and corresponding retinal histology from about 6° TR. a) An averaged AO-OCT B-scan (From Fig. 5.a.); b): Magnified view of an averaged OCT B-scan (from Fig. 5.b.); c) Magnified section of the inner retina from AO-OCT scan (From Fig. 6.a.) with corresponding retinal histology (from <http://www.bu.edu/histology/p/079020oa.htm> [10])

Despite lateral “blurring” caused by averaging of several AO-OCT B-scans, detailed inner retinal morphology can be seen in that image. Moreover different retinal layers exhibit different “granulation” and contrast of the small features within each layer. Application of B-scan averaging suggests that the “granulation” represents the scattering centers within these retinal layers and that it is not created by random speckle noise.

4. CONCLUSIONS

We have implemented an AO-OCT/AO-SLO system for extracting retinal motion data present during AO-OCT image acquisition. It is evident that volumetric AO-OCT imaging is possible only in patients with very good fixation or with very high-speed image acquisition OCT systems. Using this information we decided to focus our effort on creating averaged B-scans with reduced speckle contrast to make possible better visualization of cellular morphology of inner retina. We plan to implement this strategy in the future to image different retinal structures on both healthy and diseased subjects to further test the feasibility of this method. As a result, averaged AO-OCT B-scans should be easier to interpret for clinicians. We hope that both methods help to establish AO-OCT as a powerful clinical imaging modality. In the future additional speckle reduction methods such as angular compounding [11-12] or frequency compounding [13] will be considered to further limit speckle contrast and reduce the number of B-scans that have to be averaged.

5. ACKNOWLEDGEMENTS

We gratefully acknowledge the contributions of Scott B. Stevenson from the University of Huston and Qiang Yang, David W. Arathorn and Curtis R. Vogel from Montana State University. This research was supported by the National Eye Institute (EY 014743).

REFERENCES

- [1] K. Y. Li, P. Tiruveedhula and A. Roorda “Intersubject variability of foveal cone photoreceptor density in relation to eye length” *Invest. Ophthalmol. Vis. Sci.* 51, 6858-6867 (2010)
- [2] A. Dubra and Y. Sulai, "Reflective afocal broadband adaptive optics scanning ophthalmoscope," *Biomed. Opt. Express* 2, 1757-1768 (2011)
- [3] A. Dubra, Y. Sulai et al. "Noninvasive imaging of the human rod photoreceptor mosaic using a confocal adaptive optics scanning ophthalmoscope," *Biomed. Opt. Express* 2, 1864-1876 (2011)
- [4] R. J. Zawadzki, S. S. Choi, et al. "Adaptive optics-optical coherence tomography: optimizing visualization of microscopic retinal structures in three dimensions," *J. Opt. Soc. Am. A* 24, 1373-1383 (2007)
- [5] O. P. Kocaoglu, B. Cense, et al. "Imaging retinal nerve fiber bundles using optical coherence tomography with adaptive optics." *Vision Research* 51, 1835-44 (2011)
- [6] R.J. Zawadzki, S.M. Jones, S. Olivier, M. Zhao, B. Bower, J. Izatt, S.S. Choi, S. Laut and J.S. Werner, "Adaptive-optics optical coherence tomography for high-resolution and high-speed 3D retinal in vivo imaging," *Opt. Express* 13, 8532-8546 (2005)
- [7] R. J. Zawadzki, S. M. Jones, et al. "Integrated adaptive optics optical coherence tomography and adaptive optics scanning laser ophthalmoscope system for simultaneous cellular resolution in vivo retinal imaging," *Biomed. Opt. Express* 2, 1674-1686 (2011)
- [8] P. Thévenaz, U.E. Ruttimann, M. Unser, "A pyramid approach to subpixel registration based on intensity," *IEEE Transactions on Image Processing*, 7, 27-41 (1998)
- [9] T. Klein, W. Wieser, C.M. Eigenwillig, B.R. Biedermann, and R. Huber, "Megahertz OCT for ultrawide-field retinal imaging with a 1050nm Fourier domain mode-locked laser," *Opt. Express* 19, 3044-3062 (2011)
- [10] "A Learning System in Histology: CD-ROM and Guide" Oxford University Press (ISBN 0-19-515173-9), (2002)
- [11] N. Iftimia, B. E. Bouma, and G. J. Tearney, "Speckle reduction in optical coherence tomography by “path length encoded” angular compounding," *J. Biomed. Opt.* 8(2), 260–263 (2003)
- [12] A. E. Desjardins, B. J. Vakoc, et al. "Speckle reduction in OCT using massively-parallel detection and frequency-domain ranging," *Opt. Express* 14(11), 4736–4745 (2006)
- [13] M. Pircher, E. Gotzinger, et al. "Speckle reduction in optical coherence tomography by frequency compounding," *J. Biomed. Opt.* 8(3), 565–569 (2003)